FUDMA Journal of Sciences (FJS)
ISSN online: 2616-1370
ISSN print: 2645 - 2944
Vol. 10 No. 24, December, 2026, pp 202 – 212
DOI: https://doi.org/10.33003/fjs-2026-1024-6234

Wind–Solar Climate-Resource Adequacy in Semi-Arid Iraq: Reconstructed ERA5 Diagnostics and Conditional CMIP6 Models

Safaa J. Al-Swaiedi

General Directorate of Education Al-Karkh Third, Ministry of Education, Baghdad, Iraq.

*Corresponding authors' email: safaa.jasim1992@gmail.com

Received: 14 Oct. 2026
Accepted: 10 Nov. 2026
Published: 13 Nov. 2026

ABSTRACT

Mean-resource assessments miss days when wind and PV potential are simultaneously weak. Wind–solar resource indicators were reconstructed for the Al-Shahabi region in southeastern Iraq using 227,928 hourly ERA5 time steps across 12 grid cells during 1995–2020. Conditional resource responses were subsequently assessed using five CMIP6 models under SSP2-4.5 and SSP5-8.5.WPD is calculated from hourly 100 m wind vectors and air density; a temperature-adjusted PV proxy is derived from hourly horizontal irradiation. Historical 20th-percentile (P20) thresholdsdefine comparable low resource days. The mean wind power density was 296.74 W m^{-2}, while the mean daily temperature-adjusted PV resource indicator was 0.7508 kWh m^{-2} d^{-1}. Simultaneous deficiencies occur on 643/9497 (6.77%) days, mostly in boreal winter. For four future scenario–horizon combinations, the equal-weight five-model mean WPD changes −3.19% to −6.98% (all five models are reduced under transfer assumptions), while concurrent low-resource frequency changes range from −0.20 to +0.63 percentage points (pp) in the ensemble mean and are not signed consistently among individual models. Sensitivity analyses show strong seasonality dependence of thresholds and wind change amplitude transferred. These results separate a relatively coherent mean wind-resource response from much less robust compound-deficitbehaviour. Because monthly change signals are imposed on historical sequences, the adjusted daily episodes are conditional threshold outcomes but not predictions for weather persistence or operational electricity system reliability.

Keywords: Wind Power Density, Photovoltaic Resource Potential, CMIP6, ERA5, Climate Change.

INTRODUCTION

Wind and solar cannot be climate-resiliently assessed only on annual resource averages. Electricity-system stress is not just how many renewable resources there are but when, where and for how long unusually low availability conditions occur; wind–solar complementarity and renewable energy drought studies therefore increasingly take temporal correlations, threshold events and simultaneous shortages into account(Bracken et al., 2024; Li et al., 2024; Wilczak et al., 2024). They are useful screening tools for potential resource but meteorological deficiency must not be equated with unserved electricity without taking installed technologies into account (demand, storage and network operation) as well (Morin et al., 2025; Wilczak et al., 2024).

Climate change makes this even more difficult. Changes in wind speed can have disproportionately large effects on the available atmospheric kinetic flux since WPD is a cube of velocity; PV performance depends on insolation and module temperature; rising ambient temperature may reduce part of benefit from otherwise favourable irradiance(Bhatt et al., 2022; Skoplaki & Palyvos, 2009). CMIP6 combines historical and scenario experiments but multi-model projections introduce uncertainty due to spatial resolution, circulation biases, experiment members and scenario dependent regional responses(Chen & Ji, 2024; Eyring et al., 2016; O'Neill et al., 2016; Tebaldi et al., 2021). Any claim about changing compound shortages must therefore be explicit about how daily weather variability has been represented.

Previous studies have highlighted the importance of assessing renewable-energy resource adequacy beyond conventional long-term mean indicators. Bracken et al. (2024) established a standardized framework for evaluating historical compound wind–solar energy droughts across the contiguous United States, while Li et al. (2024) investigated the relationships among renewable-resource availability, temporal variability, and coincident scarcity. Subsequently, Bracken et al. (2025) examined the combined influence of climate change and evolving energy infrastructure on renewable-energy droughts in the western United States(Bracken et al., 2025). In the European context, Kapica et al. (2024) assessed the potential effects of climate change on renewable-energy droughts, highlighting their spatially heterogeneous responses(Kapica et al., 2024). Furthermore, Morin et al. (2025) demonstrated the importance of wind–solar resource combinations in characterising renewable-energy droughts. Complementarity assessments have also been advanced through studies examining the temporal relationships between wind and solar resources(Costoya et al., 2023; Pedruzzi et al., 2023). Collectively, these investigations emphasize the importance of evaluating resource variability and compound low-resource conditions alongside changes in mean renewable-energy potential.

The regional context is important. Iraq has high insolation but a heterogeneous wind resource and previous Iraq specific analyses have looked at temporal complementarity of wind–solar resources using gridded climatic and land cover data(Sachit et al., 2022). That evidence does not establish by itself how a fixed historical threshold of coincident lower tail resources would react to future change signals; nor can assessments done in Europe or North America establish the statistical behaviour of semi-arid southeastern Iraq. In the

1absence of long-term, site-specific ground-based measurements suitable for independent validation, particular attention must be given to the transparency, physical consistency, and reproducibility of reanalysis-based resource assessments. Although ERA5 provides a comprehensive representation of atmospheric conditions, uncertainties associated with spatial resolution, model parameterizations, and observational constraints may affect the accuracy of locally derived wind and solar resource indicators (Hersbach et al., 2020; Wilczak et al., 2024). Accordingly, the present study explicitly documents its computational assumptions, applies consistent temporal and spatial aggregation procedures, and evaluates the sensitivity of the principal resource-adequacy indicators to selected methodological choices.

This study asks a testable question: does the direction of projected change in average wind resource persist with respect to the direction of change in simultaneous low wind–solar exposure? The contribution is hourly reconstruction of the common historical baseline, separate diagnostics for wind-resource magnitude, thermally adjusted solar potential, fixed quantile coincidence, episode structure and sensitivity to assumptions about future transfer. The objectives of this study were to (i) reconstruct historical ERA5 resource indicators, (ii) quantify seasonal and compound low-resource exposure, (iii) assess responses to five CMIP6 models under two emission pathways, and (iv) evaluate key methodological sensitivities and limitations. What we study are climate-resource adequacy indicators not operational reliability of a particular hybrid plant.

MATERIALS AND METHODS

Study Area and Input Datasets

The study area is centred nominally at 32.20°N, 45.90°E in Al-Shahabi of Wasit Governorate in southeastern Iraq; ERA5 evaluation grid is 32.00–32.50°N and 45.50–46.25°E (in both coordinates by 0.25°) so analysis is done over 12 cells. The historical analysis covered 1 January 1995 to 31 December 2020, comprising 227,928 hourly UTC time steps and 9,497 calendar days, including leap days. Each of the 12 ERA5 grid cells contained a complete hourly record, yielding 2,735,136 cell-hour observations per meteorological variable. This spatiotemporally complete dataset provided the basis for calculating the historical wind and solar resource indicators. ERA5 variables retained were zonal and meridional 100 m winds u100 and v100, 2 m temperature T2m, surface pressure sp and surface solar radiation downwards ssrd. ERA5 is a global atmospheric reanalysis that combines model information with assimilated observations; it does not constitute direct station-based measurements at the study site (Hersbach et al., 2020).

Five CMIP6 models were selected for matched data records (BCC-CSM2-MR, GFDL-ESM4, MPI-ESM1-2-LR, MRI-ESM2-0 and NorESM2-MM); historical reference is 1995–2014; future scenario windows are 2031–2060 and 2071–2100 under SSP2-4.5 and SSP5-8.5 respectively. The CMIP6 variables required are near surface air temperature (tas), near surface wind speed (sfcWind), surface air pressure (ps) and surface downwelling shortwave radiation (rsds). These data were retrieved from ESGF and matched by model, scenario, experiment member and location within each model. The two SSP pathways follow ScenarioMIP experiment framework(O'Neill et al., 2016; Tebaldi et al., 2021). They are used to denote different forcing trajectories rather than probabilities of occurrence.

All five CMIP6 selections have required temporal coverage (no missing extracted values), but the models have different native grids and calendars. Table 1 shows extracted native-cell centres and their distance from nominal study centre. The consistency of model files does not imply representativity: some selected centres are about 89–98 km from nominal reference point (offsets are treated explicitly as limitations rather than negligible).

Table 1: Extracted CMIP6 Native-grid Locations, Offsets from the Nominal Al-Shahabi Centre, and Native Calendar Types

Model	Latitude (°N)	Longitude (°E)	Offset (km)	Calendar
BCC-CSM2-MR	31.9624	46.1250	33.9	365_day
GFDL-ESM4	32.5000	45.6250	42.2	noleap
MPI-ESM1-2-LR	32.6420	45.0000	97.7	proleptic_gregorian
MRI-ESM2-0	31.9624	45.0000	88.8	proleptic_gregorian
NorESM2-MM	32.5131	45.0000	91.4	noleap

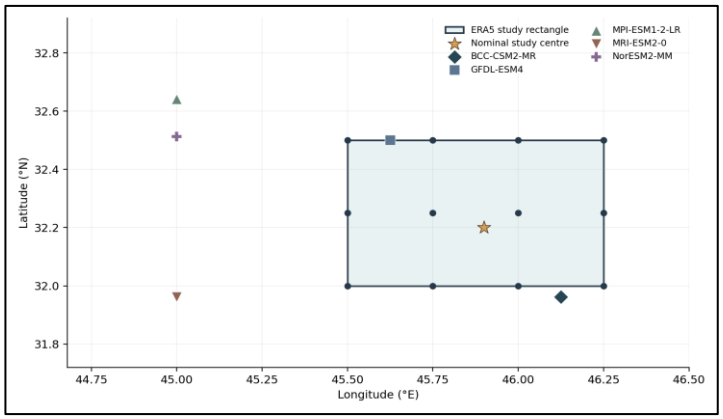


Figure 1: Geographic locations of the 12 ERA5 cells, nominal study centre, and selected CMIP6 cells. This is a coordinate schematic, not a terrain or administrative map.

All CMIP6 processing was done in each model's native time representation. Where possible daily fields were first summarised into month-specific climatologies respecting the calendar of the model; monthly fields were used immediately after variable units and coverage check was made. Only climatological climate-change factors (no splicing of individual 360 day or no leap CMIP6 calendar days into Gregorian ERA5 sequence) were transferred to ERA5 (input checks and transformation sequence are given below and summarized in Figure 2).

Hourly Wind Kinetics and the Daily Wind-Resource Index

The ERA5 velocity input is horizontal vector. Magnitude at each UTC hour and cell was computed from zonal and meridional components Eq. (1):

$$V_{100}(h,g) = \sqrt{u_{100}^2(h,g) + v_{100}^2(h,g)} \quad (1)$$

The air-density estimate in Eq. (2) is an ideal gas approximation of dry air with variables available at single levels in ERA5:Ps surface pressure Pa, T_{2m} ambient temperature K and R_d=287.05 J kg^{-1} K^{-1}dry-air gas constant (Floors & Nielsen, 2019). Moisture effects were neglected, and surface conditions used to approximate density at the 100 m assessment height introduced physical approximation error.

$$\rho(h,g) = \frac{p_s(h,g)}{R_d\, T_{2m}(h,g)} \quad (2)$$

The kinetic-energy flux per unit swept area was then derived from Eq. (3) rather than extrapolated from a turbine manufacturer's conversion curve. Density and velocity factors were paired at the same original hour and cell. Because WPD depends cubically on wind speed, the mean of hourly wind power density cannot, in general, be obtained by cubing the mean wind speed.

$$\mathrm{WPD}(h,g) = \frac{1}{2}\rho(h,g)\, V_{100}^3(h,g) \quad (3)$$

For a whole UTC Day, hourly WPD was averaged over 24 hours and cells equally weighted Eq. (4). Units are W m^{-2}. Each cell contributed equally; no turbine site weighting, installed capacity weighting or electricity demand weighting was applied:

$$\overline{\mathrm{WPD}}_d = \frac{1}{24N_g}\sum_{g=1}^{N_g}\sum_{h\in d}\mathrm{WPD}\,(h,g) \quad (4)$$

Solar Irradiation and the Photovoltaic Resource Proxy

The ERA5 variable ssrd is accumulated downward shortwave energy incident on a horizontal surface. The archived hourly samples used here represent one-hour accumulations in J m^{-2}. Equation (5) converts the non-negative accumulated energy $E_{h,g} = \max(\mathrm{ssrd}_{h,g}, 0)$ to mean irradiance $G_{h,g} = E_{h,g}/3600$W m^{-2} and one-hour irradiation $H_{h,g} = E_{h,g}/(3.6\times10^6)$kWh m^{-2}. Values below zero were set to zero as physically invalid accumulated insolation. The appropriate temporal accumulation interval is essential when interpreting ERA5 ssrd and should be confirmed in the archived hourly product metadata(Copernicus Climate Change Service, 2018).

$$G_{h,g} = \frac{E_{h,g}}{3600}, \quad H_{h,g} = \frac{E_{h,g}}{3.6\times10^6} \quad (5)$$

Then daily global horizontal irradiation was calculated as $\mathrm{inGHI}_d = N_g^{-1}\sum_g\sum_{h\in d}H_{h,g}$, kWh m^{-2} d^{-1}. This is a resource of the horizontal plane. It cannot be identified with tilted-array irradiance without transposition assumptions. Instead of electrical plant output, we used a temperature-adjusted resource proxy(Pantic et al., 2016; Skoplaki & Palyvos, 2009). In Eq. (6), T_{2m} in K is converted to °C; NOCT = 45°C is declared, and conventional reference conditions are ambient temperature 20°C and irradiance 800 W m^{-2}.

$$T_{\mathrm{cell}}(h,g) = T_{2m}(h,g) - 273.15 + \frac{\mathrm{NOCT}-20}{800}\,G_{h,g} \quad (6)$$

Temperature-corrected PV conversion was estimated at the same hourly time resolution as irradiation. Eq. (7) defines the daily proxy as irradiance integrated against a linear temperature correction:$\eta_{\mathrm{ref}} = 0.15$, $\gamma = 0.004\ ^\circ\mathrm{C}^{-1}$, and $T_{\mathrm{ref}} = 25\ ^\circ\mathrm{C}$. These are declared assumptions not calibrated properties of an Iraqi PV module. The references justify general form of cell-temperature/efficiency relationships but do not test coefficients at sitestudy (Pantic et al., 2016; Skoplaki & Palyvos, 2009):

$$\mathrm{PV}_d = \frac{\eta_{\mathrm{ref}}}{N_g}\sum_{g=1}^{N_g}\sum_{h\in d}H_{h,g}\,[1-\gamma(T_{\mathrm{cell}}(h,g)-T_{\mathrm{ref}})] \quad (7)$$

The daily temperature-adjusted photovoltaic resource indicator defined in Eq. (7) is expressed in kWh m^{-2} d^{-1} per unit of nominal module area. By integrating hourly irradiation with the corresponding temperature-dependent conversion efficiency, the formulation preserves the temporal co-variability between solar irradiance and estimated cell temperature. Nevertheless, the adopted model represents an idealized photovoltaic resource approximation rather than the electrical output of a specific PV installation. It does not explicitly account for module tilt and orientation, irradiance transposition, wind-dependent convective cooling, technology-specific electrical characteristics, shading, soiling, degradation, inverter clipping, wiring losses, or other balance-of-system effects. Accordingly, the resulting indicator is employed to assess relative variations in photovoltaic resource potential under historical and climate-adjusted conditions, without implying site-specific predictions of actual electricity generation or operational plant performance.

Monthly Climate-Signal Estimation and Transfer

For each model k, calendar month m, and future pathway–horizon combination q, historical model climatologies (1995–2014) were compared with the corresponding future climatologies (2031–2060 or 2071–2100). Equation (8) shows the multiplicative change factors for wind speed, irradiation and pressure, together with the additive temperature change. The same model member and grid cell are used in each historical–future comparison. A month-specific model climatology is constructed using its native calendar before transferring the signal to ERA5; this preserves seasonal phases while avoiding incompatible dates between 360-day, no-leap and Gregorian calendars(Eyring et al., 2016; Tebaldi et al., 2021).

$$F_{V,kqm} = \frac{\overline{\mathrm{sfcWind}}_{kqm}^{\mathrm{future}}}{\overline{\mathrm{sfcWind}}_{km}^{\mathrm{historical}}}, \quad F_{R,kqm} = \frac{\overline{\mathrm{rsds}}_{kqm}^{\mathrm{future}}}{\overline{\mathrm{rsds}}_{km}^{\mathrm{historical}}},$$
$$F_{p,kqm} = \frac{\overline{\mathrm{ps}}_{kqm}^{\mathrm{future}}}{\overline{\mathrm{ps}}_{km}^{\mathrm{historical}}}, \quad \Delta T_{kqm} = \overline{\mathrm{tas}}_{kqm}^{\mathrm{future}} - \overline{\mathrm{tas}}_{km}^{\mathrm{historical}} \quad (8)$$

The twelve-monthly signals for each variable were linearly interpolated between mid-month anchors and applied in an annual cycle to each hour of the 1995–2020 ERA5 baseline. Wind factors multiplied both horizontal wind components (thus keeping historical direction), irradiation, and surface pressure by their factors, and temperature was changed additively; hourly variables were passed back through Eqs. (1)– (7); WPD was then recomputed using adjusted density and cube of adjusted hourly wind speed. Alternatively,

piecewise constant calendar-month transfer was analysed as a sensitivity test.

Crucially, F_V is calculated from CMIP6 near-surface wind and then transferred to ERA5 100-m winds. This assumes identical fractional climate change at the two heights; it is not equivalent to independently projecting future 100-m wind shear. A sensitivity experiment modifies the departure of F_V from unity by factors of 0.5, 1.0 and 1.5 before repeating the hourly calculations. That experiment probes dependence on an assumption but cannot verify its physical correctness. Because every adjusted record follows the original ERA5 hourly ordering, the derived daily deficits represent conditional changes to historical resource exposure rather than simulated future synoptic sequences.

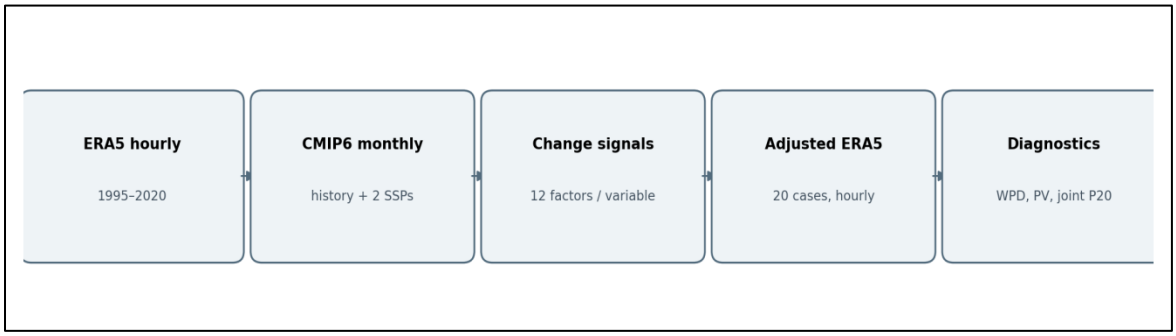


Figure 2: Auditable sequence of historical reconstruction, CMIP6 monthly change-signal derivation, hourly ERA5 adjustment and resource diagnostics.

Fixed Historical Low-Resource Thresholds and Coincidence

The main deficiency threshold for each resource was its historical ERA5 daily P20 value over the full 1995–2020 reference (constant when classifying all scenario-adjusted series). The below-threshold indicator for a resource is Eq. (9), here, X_d denotes either daily WPD or the temperature-adjusted PV resource indicator, whereas $Q_p^{\mathrm{ERA5}}(\mathrm{X})$ is the corresponding fixed historical percentile threshold. Inequalities are strict; quantiles from the empirical sample are estimated independently for the two resources. P20 is an operational definition of the lower tail, not a physically measured cut in the threshold or model of unmet demand (Bracken et al., 2024; Morin et al., 2025).

$$I_X(d;p) = \begin{cases} 1, & X_d < Q_p^{\mathrm{ERA5}}(X), \\ 0, & X_d \geq Q_p^{\mathrm{ERA5}}(X), \end{cases} \quad p = 0.20 \tag{9}$$

Eq. (10) expresses simultaneous low-resource exposure and its complement, the resource adequacy index. The latter is, by design, a day-count complement and does not have the probabilistic meaning of generation adequacy in a load-serving system. Episode length is run over calendar days satisfying both indicators. The seasonal analysis follows the conventional classification: DJF (winter), MAM (spring), JJA (summer), and SON (autumn); all dates are UTC.

$$J(d) = I_W(d;0.20)I_S(d;0.20),$$
$$f_{WS} = \frac{1}{N_d}\sum_{d=1}^{N_d} J(d), \quad R_{WS} = 1 - f_{WS} \tag{10}$$

Two sets of sensitivity analyses were performed: fixed historical thresholds at P10, P15, P25 and P30 and seasonality adjusted alternative based on month of year historical P20 thresholds. These tests are needed since interpretation of one all-year solar threshold can be dominated by winter irradiance; the fixed-threshold experiment compares with a reference not unconditional frequency of meteorological drought in a newly simulated future climate.

Complementarity was defined separately from threshold coincidence. Pearson correlation coefficient between paired daily WPD and PV proxy is transformed in Eq. (11) into bounded index CI ∈ [0,1]. The normalized index, CI=(1-r)/2, is a linear transformation of the Pearson correlation coefficient and does not independently quantify operational complementarity; it does not prove statistical independence r=0 or quantify storage and dispatch benefits (Pedruzzi et al., 2023).

$$\mathrm{CI} = \frac{1-r(\overline{\mathrm{WPD}}_d, \mathrm{PV}_d)}{2} \tag{11}$$

Statistical Diagnostics, Ensemble Interpretation and Reproducibility

Historical annual means of WPD, PV proxy, GHI and air temperature were tested for two-sided Kendall rank trend(Kendall, 1938; Mann, 1945) and median pairwise slopes by Theil–Sen(Sen, 1968). Annual lag one correlation was checked but values reported are not adjusted for temporal autocorrelation so should not be taken as exhaustive test of trend under correlated climate variability. For future summaries each model counts once. Inter-model standard deviations report only spread among five models (not 95% confidence intervals or internal variability uncertainty); agreement counts, minima and maxima are given separately. Leave-one-model-out means test whether ensemble conclusions dominated by single selected model. Ensemble is not weighted by locally calibrated skill score because no credible independent observational benchmark exists for all variables and locations.

NASA POWER is noted as a second gridded source (not ground-based validation). The previously reported quantitative ERA5–NASA POWER comparisons could not be independently reproduced from the available matched inputs and were therefore excluded from the revised results. Numerical provenance records source files, grid point coordinates, calendar conventions, monthly transfer factors and individual model outputs needed to reproduce calculations.

RESULTS AND DISCUSSION

Reconstructed 1995–2020 Wind and Photovoltaic Resource Climatology

The reconstructed ERA5 record has no missing UTC hours in the analysis variables. Domain-mean 100 m wind speed is 6.739 m s^{-1}; hourly-calculated WPD mean is 296.743 W m^{-2} (Table 2). Mean air density (dry-air approximation) is 1.1725 kg m^{-3}. Mean daily GHI is 5.6607 kWh m^{-2} d^{-1}, temperature adjusted PV proxy is 0.7508 kWh m^{-2} d^{-1} with nominal efficiency of 15% specified and module temperature

response. These figures should not be confused: GHI measures irradiation at the surface, while the PV proxy is scaled by a simplified conversion efficiency that depends on temperature. Different units of interpretation are needed to have a physically coherent Results section.

Table 2: Hourly Reconstructed ERA5 Resource Indicators and Fixed Daily P20 Thresholds for 1995–2020 (12-Cell Study Domain)

Indicator	Reconstructed Value
Observation interval	1995–2020; 227,928 hourly time steps per grid cell; 12 grid cells; 9,497 days
ERA5 grid	12 equal-weight cells on 0.25° regular grid
Mean 100-m wind speed	6.739 m s^{-1}
Mean air density (dry-air proxy)	1.1725 kg m^{-3}
Mean WPD	296.743 W m^{-2}
Mean GHI	5.6607 kWh m^{-2} d^{-1}
Mean PV resource proxy	0.7508 kWh m^{-2} d^{-1}
Daily P20 WPD threshold	78.504 W m^{-2}
Daily P20 PV threshold	0.535027 kWh m^{-2} d^{-1}
Low-WPD / low-PV day counts	1,900 / 1,900
Jointly low-resource days	643 / 9,497 (6.7706%)
Resource adequacy / normalized CI	R_{WS} = 0.932294; CI = 0.377168
Contiguous joint-deficit spells	357 episodes; mean 1.80 d; maximum 9 d

At the P20 cut-off, the wind and PV proxy have 1900 individual low-resource days each. Coincidence is 643 out of 9497 (6.7706%); joint adequacy index = descriptive = 0.932294. Normalized daily correlation complementarity index = 0.377168 shows a positive linear correlation between the two daily indicators, so marginal threshold frequencies cannot be added to represent coincident scarcity: joint count tells us about paired structure of the same days, not independent deficits in wind and solar.

The historical joint-deficit events are 357 contiguous spells; mean episode length is 1.80 days and maximum nine days. These durations are the actual ERA5 sequence during the analyzed history (future counterparts based on transfer are not forecasts of future event ordering); for comparison, we also show the historical mean WPD, PV proxy, and coincident exposure (Table 3 and Fig. 3).

Table 3: Seasonally Resolved ERA5 Resource Indicators and Daily Deficits Simultaneously. Low-Resource Classification uses the same Annual P20 Thresholds in Every Season

Season	Days	WPD (W m^{-2})	PV Proxy (kWh m^{-2} d^{-1})	Joint Days	Joint (%)	CI
DJF	2347	215.22	0.517	471	20.07	0.575
MAM	2392	253.75	0.873	9	0.38	0.577
JJA	2392	479.05	0.953	0	0.00	0.348
SON	2366	236.77	0.655	163	6.89	0.378

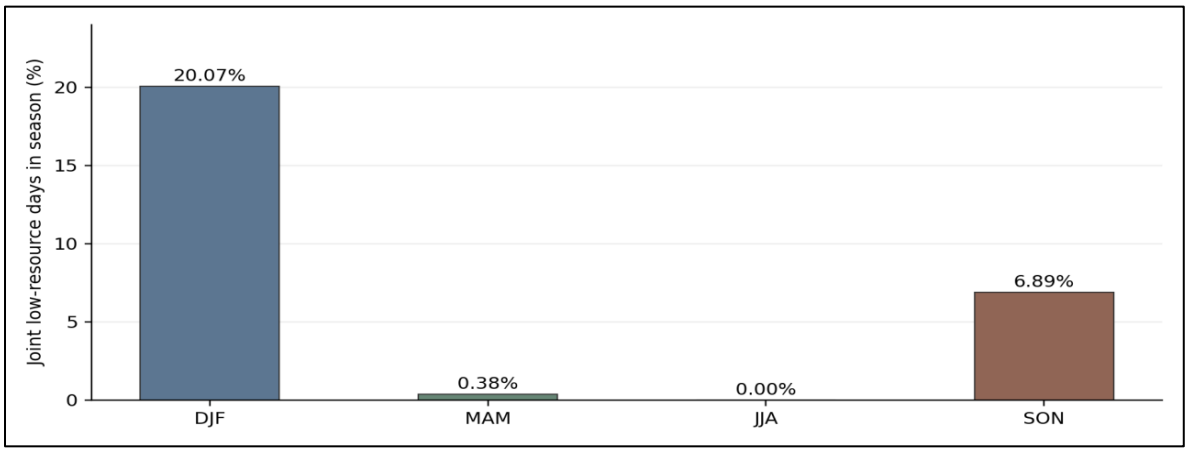


Figure 3: Fraction of days with wind and photovoltaic-resource deficiencies simultaneously classified using fixed annual ERA5 P20 thresholds. Percentages have season-specific denominators.

Of the 643 historical coincident days: 471 were DJF (73.3%), 163 SON (25.3%), nine MAM (1.4%), and none JJA. As fractions of days in each season, joint deficit frequency is 20.07%, 6.89%, 0.38%, and 0.00%. Winter concentration is partly definitional: PV output relative to an annual irradiance threshold is much lower in winter. P20 calendar month as a benchmark, the total historical joint count becomes 464 days (4.89%). The difference shows seasonal adjustment affects what's called compound deficit, not just some minor numerical refinement.

Dependence on the Historical Baseline Window and Annual Trends

A direct comparison of the two reference intervals shows a small but non-zero baseline-window effect: mean WPD 1995–2014 = 299.692 W m^{-2} vs 296.743 W m^{-2} over full 1995–2020; PV proxy values are 0.75243 and 0.75083 kWh

m^{-2} d^{-1}. With P20 full-reference cutoffs, the joint-deficit fraction is 6.46% in 1995–2014 and 6.77% over 1995–2020. These differences have to be made clear because CMIP6 historical experiment ends in 2014 while ERA5 anchor goes to 2020. The design uses the 20-year CMIP6 history to estimate within model climate factors not as an assertion that ERA5 has an observed CMIP6 historical analogue through 2020.

Annual trend tests do not provide evidence at 5% unadjusted significance level that any of the annual means analysed have changed monotonically: as summarized in Table 4 WPD has Kendall ($\tau = -0.0154$and $p = 0.9305$) and GHI and the PV proxy each return $p = 0.0704$. The latter both show negative ranked association over this record but neither an unambiguous monotonic trend once all limitations of the test are taken into account. Lag-one correlations were tested annually; nominal values have not been corrected for serial correlation and observational record is limited to 26 annual values so absence of small values should not be interpreted as evidence of stationary climate conditions.

Table 4: Mann–Kendall Trend Statistics and Theil–Sen Slope Estimates for Annual ERA5 Resource Indicators over 1995–2020

Annual indicator	Kendall's τ	p-value	Theil–Sen slope	95% slope range
WPD (W m^{-2})	−0.015	0.9305	−0.07479	[−1.26702, +0.98773]
PV proxy (kWh m^{-2} d^{-1})	−0.255	0.0704	−0.00034	[−0.00066, +0.00002]
GHI (kWh m^{-2} d^{-1})	−0.255	0.0704	−0.00241	[−0.00545, +0.00022]
T_2m (°C)	−0.138	0.3356	−0.01185	[−0.03428, +0.01148]

Table note: Theil–Sen slopes and their corresponding 95% slope ranges are expressed in the respective indicator units per year: W m^{-2} yr^{-1} for WPD, kWh m^{-2} d^{-1} yr^{-1} for the PV resource indicator and GHI, and °C yr^{-1} for air temperature. Kendall's τ is dimensionless. Reported p-values are two-sided and have not been adjusted for serial autocorrelation.

Multi-Model Changes in Mean Wind and Photovoltaic Indicators

All 20 model–scenario–horizon calculations were done with hourly adjusted ERA5 inputs and future climate signals for each of the five CMIP6 models separately (Table 5 gives equal-weight averages across all five model responses for each scenario–horizon case; Table 6 gives individual model results). The reported future periods are those of the CMIP6 climatological change-signal windows but each adjusted daily series is of length and ordering as the 9,497 day historical ERA5 anchor.

Table 5: Ensemble-Mean Changes in Wind Power Density, Photovoltaic Resource Potential, and Simultaneous Low-Resource Frequency under CMIP6 Climate-Change Scenarios

Scenario	Projection period	WPD change (%)	PVout change (%)	Joint-deficit change (pp)
SSP2-4.5	2031–2060	−3.19 ± 1.71	−1.25 ± 0.39	+0.57 ± 0.50
SSP2-4.5	2071–2100	−3.81 ± 2.01	−0.64 ± 0.48	−0.20 ± 0.80
SSP5-8.5	2031–2060	−4.23 ± 2.78	−1.33 ± 0.51	+0.33 ± 0.42
SSP5-8.5	2071–2100	−6.98 ± 3.21	−2.10 ± 0.68	+0.63 ± 0.85

Table note: Values represent the equal-weight ensemble mean ± inter-model sample standard deviation (SD) across five CMIP6 models. WPD and PVout changes are expressed as percentages relative to the historical ERA5 baseline (1995–2020), whereas changes in simultaneous low-resource frequency are expressed in percentage points (pp). Future responses are conditional on monthly CMIP6 change signals applied to the historical ERA5 hourly sequence. The reported SD describes inter-model spread and should not be interpreted as a 95% confidence interval.

Under change-signal transfer the ensemble mean WPD change is −3.195% near term SSP2–4.5; −3.810% far term SSP2–4.5; −4.234% near term SSP5–8.5 and −6.982% far term SSP5–8.5 in each of these four cases five out of five models give a negative hourly derived mean WPD change. The magnitude of the projected WPD response varied substantially among the five CMIP6 models, despite their agreement on the direction of change under the adopted transfer assumptions. So this agreement in sign should not be presented as negligible uncertainty in magnitude or formally established significant trend.

The PV proxy decreases by −1.248%, −0.642%, −1.328% and −2.098% in the four five-model summaries respectively (these changes sum CMIP6 radiation factor effect with temperature dependent efficiency assumption so they are not solely warming related). They also don't give absolute output predictions for a module. In at least one far-term pathway–horizon case across models PV response is less uniform than WPD. These differences arise because WPD depends on the cubic wind-speed response, whereas the PV indicator reflects the combined effects of irradiation and temperature-dependent conversion efficiency.

Table 6A: Individual Model Changes under SSP2-4.5 for the Two Horizons. Joint Exposure Column is Change Relative to 6.7706% Historical Coincidence; WPD and PV Changes are Relative Percentages

Signal window	Model	WPD Δ (%)	PV Δ (%)	Joint Δ (pp)	Joint days
2031–2060	BCC-CSM2-MR	-1.54	-1.74	+0.453	686
2031–2060	GFDL-ESM4	-5.69	-1.38	+0.390	680
2031–2060	MPI-ESM1-2-LR	-1.64	-1.18	+0.179	660
2031–2060	MRI-ESM2-0	-3.66	-0.65	+0.379	679
2031–2060	NorESM2-MM	-3.45	-1.29	+1.443	780
2071–2100	BCC-CSM2-MR	-0.75	-0.89	-0.653	581
2071–2100	GFDL-ESM4	-3.90	-0.50	-0.632	583

Signal window	Model	WPD Δ (%)	PV Δ (%)	Joint Δ (pp)	Joint days
2071–2100	MPI-ESM1-2-LR	-4.63	-1.23	+0.811	720
2071–2100	MRI-ESM2-0	-6.25	+0.06	-1.021	546
2071–2100	NorESM2-MM	-3.52	-0.65	+0.505	691

Table 6B: Individual Model Changes under SSP5-8.5 for the Two Projection Horizons; Definitions are as in Table 6A

Signal window	Model	WPD Δ (%)	PV Δ (%)	Joint Δ (pp)	Joint days
2031–2060	BCC-CSM2-MR	-4.40	-1.90	+0.074	650
2031–2060	GFDL-ESM4	-4.16	-1.10	+0.126	655
2031–2060	MPI-ESM1-2-LR	-7.88	-1.62	+0.579	698
2031–2060	MRI-ESM2-0	-4.65	-0.59	-0.084	635
2031–2060	NorESM2-MM	-0.08	-1.43	+0.937	732
2071–2100	BCC-CSM2-MR	-3.64	-1.50	-0.274	617
2071–2100	GFDL-ESM4	-8.60	-2.61	+0.579	698
2071–2100	MPI-ESM1-2-LR	-10.10	-2.37	+1.232	760
2071–2100	MRI-ESM2-0	-9.18	-1.26	-0.095	634
2071–2100	NorESM2-MM	-3.40	-2.76	+1.716	806

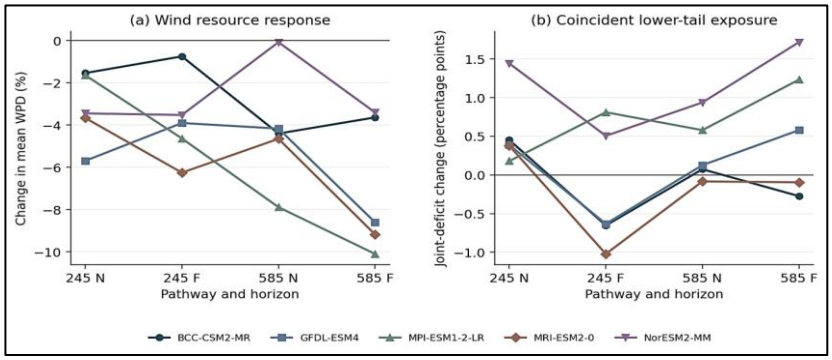


Figure 4: Responses of individual CMIP6 models to (a) mean WPD (%) and (b) simultaneous low-resource exposure (percentage points, pp). N and F denote near (2031–2060) and far (2071–2100) signal windows respectively. Lines connect different scenario–horizon cases only to improve model identification; horizontal axis is not continuous time.

The comparison is between consistent decrease in mean WPD and non-uniform coincidence response. Equal-weight joint frequency changes are +0.569 pp (SSP2-4.5 near), −0.198 pp (SSP2-4.5 far), +0.326 pp (SSP5-8.5 near), and +0.632 pp (SSP5-8.5 far). All 5 models predict increased coincidence in SSP2-4.5 near term. Agreement loosens in far terms: SSP2-4.5 far has two increases and three decreases; SSP5-8.5 far has three increases and two decreases. Under SSP2-4.5 far, this gives a small negative mean change, though ensemble mean WPD decreases. This answers the central research question: shifts in wind-resource magnitude vs joint lower-tail threshold exposure are not interchangeable metrics.

Threshold, Wind-Height and Model-Selection Sensitivity

The alternative P10, P15, P25 and P30 classifications were recomputed with their own fixed historical thresholds. The magnitude and, in some cases, the direction of the joint-deficit response depend on the selected percentile threshold. Choice of P20 is therefore transparent and reproducible but not privileged by physics. More sensitivity should be expected when many paired daily values are near chosen cut-offs; ERA5 ordering itself is preserved.

Table 7: Ensemble-Mean Changes in Joint Low-Resource Exposure (Percentage Points) under Alternative Fixed Historical Percentiles

Threshold	245 near (pp)	245 far (pp)	585 near (pp)	585 far (pp)
P10	+0.230	-0.011	+0.137	+0.280
P15	+0.463	-0.032	+0.255	+0.583
P20	+0.569	-0.198	+0.326	+0.632
P25	+0.849	+0.027	+0.545	+0.853
P30	+0.611	-0.152	+0.512	+0.800

A second sensitivity test multiplied the transferred fractional near-surface wind change by multipliers 0.5, 1.0 and 1.5; in all twelve aggregated pathway–horizon–multiplier combinations five-model average WPD response was negative. SSP5-8.5 far term three mean WPD responses are −4.45%, −6.98% and −9.30% as wind change amplitude increases. These tests show that the direction of ensemble-mean WPD response within the specified transfer family is robust, but not that future change at 100 m follows any of those assumed amplitudes. The leave-one-model-out range crosses zero, indicating that the sign of the ensemble-mean

joint-deficit response is sensitive to model selection and should not be interpreted as robus

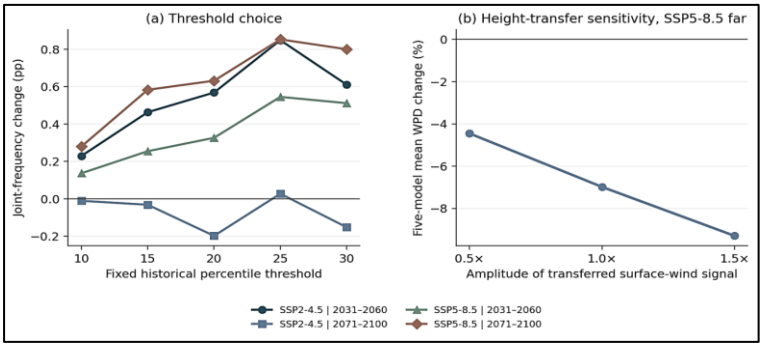


Figure 5: Low-resource exposure to fixed historical thresholds (left) and far-term SSP5-8.5 mean WPD sensitivity to amplitude of transferred near-surface wind climate signal (right). All values plotted are recalculated from scenario-adjusted reference series

Episode Characteristics and NASA POWER Comparison Scope

With the full historical daily sequence 643 joint-deficit days are identified as episodes of at least one day (mean spell length = 1.80 days and maximum nine). For each modified scenario we can count an equivalent episode counter (Tables 6A–6B give day counts) but these episodes are mechanically affected by smooth monthly factors applied to ERA5 ordering so their apparent difference in duration cannot be used as independent model predictions of future synoptic persistence, blocking patterns or extreme event clustering. This restriction is important when research wants to inform storage/backup sizing(Morin et al., 2025; Wilczak et al., 2025).

NASA POWER was an external comparison source in the earlier manuscript. POWER has gridded surface meteorological and solar parameters useful for ERA5 (National Aeronautics and Space Administration, n.d.) but is not a local flux tower or pyranometer nor physically independent ground truth for ERA5. Comparisons at unequal wind measurement heights are especially inappropriate for direct bias interpretation. Since the inherited quantitative comparison could not be independently reproduced with fully matched inputs numerical NASA POWER validation claims are deliberately left out of this revised evidence-based account. Independent station verification would materially strengthen resource magnitude estimates and bounds on uncertainty.

Discussion

Mean Wind-Resource Changes and Compound Low-Resource Exposure

The results show that changes in mean wind-resource availability do not necessarily translate into corresponding changes in simultaneous wind–solar deficits. Across the four scenario–horizon combinations, the equal-weight ensemble-mean wind power density (WPD) decreased by 3.19–6.98% relative to the historical ERA5 baseline. All five selected CMIP6 models produced negative WPD responses under the adopted change-signal transfer assumptions, although the magnitudes varied appreciably among models. The consistency of this directional response contrasts with the less uniform behaviour of compound low-resource exposure.

Changes in the ensemble-mean frequency of simultaneous deficits ranged from −0.20 to +0.63 percentage points. Under SSP2-4.5 for 2031–2060, all five models indicated an increase in joint-deficit frequency. However, the far-future SSP2-4.5 response was less consistent: two models indicated an increase and three indicated a decrease, producing a small negative ensemble-mean change. Similarly, the far-future SSP5-8.5 response differed in direction among individual models. These findings indicate that the projected reduction in mean WPD is more directionally consistent than the corresponding change in compound low-resource frequency.

The distinction arises from the different mathematical properties of the indicators. WPD is proportional to the cube of wind speed and is therefore particularly sensitive to changes in the wind-speed distribution. By contrast, the compound-deficit metric identifies days on which both wind and photovoltaic (PV) resource indicators fall below their respective historical thresholds. Its response depends not only on changes in individual resource magnitudes but also on the position of daily values relative to those thresholds and on the temporal association between the two resources. Consequently, a reduction in mean wind-resource availability does not, by itself, establish that simultaneous low-resource conditions will become more frequent.

This interpretation is consistent with the broader distinction between resource magnitude, temporal variability, and coincident scarcity discussed by Li et al. (2024). The compound-drought framework developed by Bracken et al. (2024) likewise supports treating simultaneous resource deficiencies as a separate diagnostic rather than inferring them from annual resource averages. The present results extend this line of investigation to a semi-arid region of southeastern Iraq, while remaining conditional on the selected climate models and the adopted method of transferring future climate-change signals.

Seasonality, Threshold Selection, and Wind–Solar Complementarity

The historical analysis reveals a marked seasonal concentration of simultaneous low-resource conditions. Of the 643 jointly deficient days identified during 1995–2020 using fixed annual P20 thresholds, 471 occurred during winter (DJF), corresponding to 20.07% of all winter days. No simultaneous deficit days were identified during summer under the same threshold definition. This contrast reflects, in part, the pronounced seasonal cycle of solar irradiation: a fixed annual threshold is more frequently approached or crossed during months with relatively low solar availability.

The importance of threshold definition is demonstrated by the alternative month-specific P20 analysis. When each calendar month was evaluated against its own historical reference distribution, the number of simultaneous low-resource days

decreased from 643 (6.77%) to 464 (4.89%). These classifications address different questions. A fixed annual threshold provides a common reference for identifying days below an absolute historical resource benchmark, whereas a month-specific threshold identifies unusually weak resource conditions relative to the expected seasonal state. Neither should be interpreted as a universally applicable definition of renewable-energy drought.

The sensitivity analysis reinforces this distinction. Repeating the calculations using P10, P15, P25, and P30 thresholds altered the magnitude of the estimated joint-deficit response and, in some cases, its direction. For example, the far-future SSP2-4.5 ensemble-mean change was −0.198 percentage points at P20 but +0.027 percentage points at P25. The small magnitude and threshold dependence of this response indicate that it should not be characterized as a robust improvement or deterioration in compound resource adequacy. Consequently, conclusions regarding future low-resource exposure must be interpreted alongside the threshold definitions on which they depend.

Temporal complementarity provides an additional, but distinct, description of the relationship between wind and solar resources. The historical normalized correlation-based complementarity index (CI) was 0.377, indicating positive linear co-variability between the paired daily WPD and PV resource indicators. This value does not quantify the probability of simultaneous deficits, nor does it establish whether a particular wind–solar installation would require less storage or backup generation. The observed seasonal differences and the clustering of historical deficit days demonstrate why correlation-based indices should be interpreted together with threshold-frequency and event-duration statistics. Previous assessments of wind–solar complementarity have similarly emphasized the importance of geographical context and temporal resolution(Costoya et al., 2023; Pedruzzi et al., 2023).

Uncertainty and Limitations of the Climate-Change Assessment

The principal uncertainty in the future assessment arises from the way CMIP6 climate-change signals are transferred to the historical ERA5 record. The monthly delta-change method preserves the original hourly ordering of the 1995–2020 reference series while modifying the magnitudes of meteorological variables according to model-specific monthly change factors. It therefore provides a controlled assessment of how historical resource conditions would respond to altered seasonal climate means. It does not independently simulate future changes in atmospheric circulation, daily variability, weather-regime persistence, or the timing of compound events.

This distinction is particularly important for interpreting low-resource episodes. The historical record contained 357 contiguous joint-deficit episodes, with a mean duration of 1.80 days and a maximum duration of nine days. These values describe the reconstructed ERA5 historical sequence. Although analogous episodes can be counted after applying future change factors, their timing remains inherited from the historical record. Changes in their apparent duration should therefore not be interpreted as independent CMIP6 predictions of future renewable-energy drought persistence. Investigating that question would require transient climate simulations capable of representing sub-monthly variability and changes in event sequencing, together with appropriate evaluation and bias-adjustment procedures.

A further uncertainty concerns the transfer of near-surface CMIP6 wind-speed changes to ERA5 winds at 100 m. Applying the same fractional change at both heights assumes that future modifications in vertical wind shear do not alter the transferred signal. This assumption is not independently established by the available model variables. The sensitivity analysis nevertheless indicates that the direction of the ensemble-mean WPD response is preserved over the tested range of wind-change amplitudes. For the far-future SSP5-8.5 case, the ensemble-mean WPD response varied from −4.45% to −9.30% as the transferred wind-change amplitude was altered, compared with −6.98% in the central calculation. Thus, the direction of the mean response was stable within the tested assumptions, while its magnitude remained sensitive to the wind-height transfer.

Spatial sampling and ensemble composition introduce additional uncertainty. The selected CMIP6 grid-cell centres are approximately 34–98 km from the nominal Al-Shahabi reference point, depending on the model. Such offsets may affect the representation of local wind regimes, surface conditions, and solar-resource variability. Moreover, the analysis uses one simulation member and one extracted grid location per model. The inter-model standard deviation therefore describes disagreement among the five selected responses; it does not represent the full uncertainty associated with internal climate variability, spatial sampling, or the wider CMIP6 ensemble (Eyring et al., 2016; Tebaldi et al., 2021). The leave-one-model-out analysis provides a useful check on ensemble dependence, but it cannot eliminate these uncertainties. In particular, the far-future SSP2-4.5 joint-deficit response remains sensitive to model selection.

The historical reference also carries uncertainty. ERA5 provides spatially and temporally consistent atmospheric fields, but its local accuracy depends on the observing network, data-assimilation system, and model representation of near-surface processes (Hersbach et al., 2020). The absence of suitable long-term ground-based measurements for independent validation limits confidence in the absolute resource estimates. NASA POWER provides a potentially useful complementary gridded dataset, but agreement between two gridded products should not be treated as station-based validation. Accordingly, quantitative comparison statistics that could not be reproduced from matched inputs were not retained in the revised analysis.

The photovoltaic indicator has its own limitations. Its calculation assumes a reference conversion efficiency of 15%, a temperature coefficient of 0.004 °C^{-1}, and a nominal operating cell temperature of 45 °C. These fixed parameters allow consistent comparisons across historical and climate-adjusted conditions but do not describe the complete behaviour of a particular PV technology or installation. The simplified thermal formulation excludes several installation-dependent processes, including wind-driven cooling and mounting configuration, while the resource indicator excludes electrical and balance-of-system losses. Established PV modelling studies have shown that the relationship between module temperature and electrical performance depends on the selected thermal and efficiency formulations (Skoplaki&Palyvos, 2009; Pantic et al., 2016). Consequently, the reported PV changes should be interpreted as responses of the specified resource proxy, not predictions of electricity production from an installed PV plant.

Regional Significance and Implications for Renewable-Energy Assessment

The study provides a site-focused assessment of wind–solar resource adequacy in southeastern Iraq by combining reconstructed hourly resource indicators with five model-specific climate-change responses. Earlier work on Iraq

examined the temporal complementarity of wind and solar resources using gridded climate information and land-cover products (Sachit et al., 2022). The present analysis addresses a related but more specific question: whether changes in mean renewable-resource magnitude are accompanied by changes in the frequency of simultaneous low-resource days when fixed historical thresholds are retained.

The findings have two practical implications for subsequent resource-assessment studies. First, the directionally consistent reduction in ensemble-mean WPD under the tested climate-change signals warrants attention in future wind-resource screening, although its magnitude remains conditional on the wind-height transfer assumption and spatial representation of the models. Second, the strong seasonal dependence and threshold sensitivity of compound deficits indicate that annual averages alone are insufficient to characterize the temporal availability of complementary wind and solar resources.

These results should not be interpreted as an assessment of the operational adequacy of a proposed hybrid power plant. Estimating electricity-generation reliability would require turbine power curves, technology-specific PV performance models, installed-capacity ratios, demand profiles, storage and backup configurations, and dispatch and network constraints. Studies that explicitly account for wind–solar combinations and energy-system characteristics demonstrate the importance of these additional factors when evaluating renewable-energy droughts and their consequences (Morin et al., 2025; Wilczak et al., 2025).

Accordingly, the contribution of the present study is best understood as a reproducible climate-resource screening assessment. It identifies differences between mean-resource change and simultaneous lower-tail exposure, quantifies their sensitivity to methodological choices, and provides a basis for more detailed observational, technological, and energy-system investigations in Iraq.

Conclusions

This study reconstructed hourly wind and solar resource indicators for the Al-Shahabi region of southeastern Iraq using ERA5 data for 1995–2020 and assessed their conditional responses to monthly climate-change signals from five CMIP6 models under SSP2-4.5 and SSP5-8.5.

The historical analysis yielded a mean WPD of 296.74 W m^{-2} and a mean daily temperature-adjusted PV resource indicator of 0.7508 kWh m^{-2} d^{-1}. Using fixed historical P20 thresholds, simultaneous low-resource conditions occurred on 643 of 9,497 days (6.77%), with a pronounced winter concentration and a maximum contiguous duration of nine days. Applying month-specific P20 thresholds reduced the historical joint-deficit count to 464 days (4.89%), demonstrating the influence of seasonal reference conditions on the classification of compound resource deficiencies.

Across the four scenario–horizon combinations, the equal-weight ensemble-mean WPD decreased by 3.19–6.98%, with all five selected models indicating a negative response under the adopted transfer assumptions. In contrast, changes in simultaneous low-resource frequency ranged from −0.20 to +0.63 percentage points and were not consistently signed across individual models. Sensitivity analyses further showed that conclusions concerning compound-deficit exposure depend on threshold selection and ensemble composition, whereas the negative ensemble-mean WPD response persisted across the tested wind-change amplitudes.

The principal conclusion is that projected changes in mean wind-resource availability cannot be used alone to infer changes in compound wind–solar resource adequacy. Both resource magnitude and simultaneous lower-tail exposure need to be evaluated, with explicit attention to seasonal variation and methodological uncertainty. Because the climate-change signals were applied to the historical ERA5 sequence, the results represent conditional resource responses rather than independent predictions of future drought persistence or operational power-system reliability.

Further work should prioritize independent meteorological validation, improved representation of hub-height wind changes, and transient climate simulations that resolve submonthly variability. Coupling these advances with technology-specific generation models and electricity-demand information would allow the present resource-level findings to be evaluated in an operational energy-system context.

Data and Code Availability

The ERA5 reanalysis data used in this study are publicly accessible through the Copernicus Climate Data Store (CDS; https://doi.org/10.24381/cds.adbb2d47), while the CMIP6 historical simulations and future climate projections are available through the Earth System Grid Federation (ESGF). To support computational transparency and reproducibility, the analysis was conducted using documented data-processing procedures, model-specific climate-change factors, and consistent statistical and physical formulations. The supporting computational materials, including analysis scripts, processed datasets, monthly climate-change factors, and supplementary numerical results, are maintained by the corresponding author and are available upon reasonable request.

REFERENCES

Bhatt, U. S., Carreras, B. A., Barredo, J. M. R., Newman, D. E., Collet, P., & Gomila, D. (2022). The potential impact of climate change on the efficiency and reliability of solar, hydro, and wind energy sources. *Land*, *11*(8), 1275. https://doi.org/10.3390/land11081275

Bracken, C., Voisin, N., Burleyson, C. D., Campbell, A. M., Hou, Z. J., & Broman, D. (2024). Standardized benchmark of historical compound wind and solar energy droughts across the Continental United States. *Renewable Energy*, *220*, 119550. https://doi.org/10.1016/j.renene.2023.119550

Bracken, C., Voisin, N., Mongird, K., Burleyson, C. D., & Oikonomou, K. (2025). Intensifying renewable energy droughts in the Western US amid evolving infrastructure and climate. *Earth's Future*, *13*(6), e2024EF005313. https://doi.org/10.1029/2024EF005313

Chen, G., & Ji, Z. (2024). A review of solar and wind energy resource projection based on the Earth system model. *Sustainability*, *16*(8), 3339. https://doi.org/10.3390/su16083339

Copernicus Climate Change Service. (2018). *ERA5 hourly data on single levels from 1940 to present* [Data set]. https://doi.org/10.24381/cds.adbb2d47

Costoya, X., Decastro, M., Carvalho, D., & Gómez-Gesteira, M. (2023). Assessing the complementarity of future hybrid wind and solar photovoltaic energy resources for North America. *Renewable and Sustainable Energy Reviews*, *173*, 113101. https://doi.org/10.1016/j.rser.2022.113101

Eyring, V., Bony, S., Meehl, G. A., Senior, C. A., Stevens, B., Stouffer, R. J., & Taylor, K. E. (2016). Overview of the Coupled Model Intercomparison Project Phase 6 (CMIP6) experimental design and organization. *Geoscientific Model Development*, *9*(5), 1937-1958. https://doi.org/10.5194/gmd-9-1937-2016

Floors, R., & Nielsen, M. (2019). Estimating air density using observations and re-analysis outputs for wind energy purposes. *Energies*, *12*(11), 2038. https://doi.org/10.3390/en12112038

Hersbach, H., Bell, B., Berrisford, P., Hirahara, S., Horányi, A., Muñoz-Sabater, J., Nicolas, J., Peubey, C., Radu, R., & Schepers, D. (2020). The ERA5 global reanalysis. *Quarterly journal of the royal meteorological society*, *146*(730), 1999-2049. https://doi.org/10.1002/qj.3803

Kapica, J., Jurasz, J., Canales, F. A., Bloomfield, H., Guezgouz, M., De Felice, M., & Kobus, Z. (2024). The potential impact of climate change on European renewable energy droughts. *Renewable and Sustainable Energy Reviews*, *189*, 114011. https://doi.org/10.1016/j.rser.2023.114011

Kendall, M. G. (1938). A new measure of rank correlation. *Biometrika*, *30*(1-2), 81-93. https://doi.org/10.1093/biomet/30.1-2.81

Li, M., Ma, Q., Shan, R., Abdulla, A., Virguez, E., Gao, S., & Patiño-Echeverri, D. (2024). Renewable energy quality trilemma and coincident wind and solar droughts. *Communications Earth & Environment*, *5*(1), 661. https://doi.org/10.1038/s43247-024-01850-5

Mann, H. B. (1945). Nonparametric tests against trend. *Econometrica: Journal of the econometric society*, 245-259. https://doi.org/10.2307/1907187

Morin, B., Far, A. M., Flynn, D., & Sweeney, C. (2025). Reducing RES droughts through the integration of wind and solar PV. *Renewable Energy*, *252*, 123392. https://doi.org/10.1016/j.renene.2025.123392

O'Neill, B. C., Tebaldi, C., Van Vuuren, D. P., Eyring, V., Friedlingstein, P., Hurtt, G., Knutti, R., Kriegler, E., Lamarque, J.-F., & Lowe, J. (2016). The scenario model intercomparison project (ScenarioMIP) for CMIP6. *Geoscientific Model Development*, *9*(9), 3461-3482. https://doi.org/10.5194/gmd-9-3461-2016

Pantic, L. S., Pavlović, T. M., Milosavljević, D. D., Radonjic, I. S., Radovic, M. K., & Sazhko, G. (2016). The assessment of different models to predict solar module temperature, output power and efficiency for Nis, Serbia. *Energy*, *109*, 38-48. https://doi.org/10.1016/j.energy.2016.04.090

Pedruzzi, R., Silva, A. R., Dos Santos, T. S., Araujo, A. C., Weyll, A. L. C., Kitagawa, Y. K. L., da Silva Ramos, D. N., De Souza, F. M., Narciso, M. V. A., & Araujo, M. L. S. (2023). Review of mapping analysis and complementarity between solar and wind energy sources. *Energy*, *283*, 129045. https://doi.org/10.1016/j.energy.2023.129045

Sachit, M. S., Shafri, H. Z. M., Abdullah, A. F., & Rafie, A. S. M. (2022). Combining re-analyzed climate data and landcover products to assess the temporal complementarity of wind and solar resources in Iraq. *Sustainability*, *14*(1), 388. https://doi.org/10.3390/su14010388

Sen, P. K. (1968). Estimates of the regression coefficient based on Kendall's tau. *Journal of the American statistical association*, *63*(324), 1379-1389. https://doi.org/10.1080/01621459.1968.10480934

Skoplaki, E., & Palyvos, J. A. (2009). Operating temperature of photovoltaic modules: A survey of pertinent correlations. *Renewable Energy*, *34*(1), 23-29. https://doi.org/10.1016/j.renene.2008.04.009

Tebaldi, C., Debeire, K., Eyring, V., Fischer, E., Fyfe, J., Friedlingstein, P., Knutti, R., Lowe, J., O'Neill, B., & Sanderson, B. (2021). Climate model projections from the scenario model intercomparison project (ScenarioMIP) of CMIP6. *Earth System Dynamics*, *12*(1), 253-293. https://doi.org/10.5194/esd-12-253-2021

Wilczak, J. M., Akish, E., Capotondi, A., & Compo, G. P. (2024). Evaluation and bias correction of the ERA5 reanalysis over the United States for wind and solar energy applications. *Energies*, *17*(7), 1667. https://doi.org/10.3390/en17071667

Wilczak, J. M., Kirk-Davidoff, D. B., Bloomfield, H., Bracken, C., & Sharp, J. (2025). Wind and solar energy droughts: Potential impacts on energy system dynamics and research needs. *Journal of Renewable and Sustainable Energy*, *17*(2), 022301. https://doi.org/10.1063/5.0253058

©2026 This is an Open Access article distributed under the terms of the Creative Commons Attribution 4.0 International license viewed via https://creativecommons.org/licenses/by/4.0/ which permits unrestricted use, distribution, and reproduction in any medium, provided the original work is cited appropriately.